Journal of Cerebral Blood Flow & Metabolism (2015) 35, 1358–1367

www.jcbfm.com

ORIGINAL ARTICLE

Altered contralateral sensorimotor system organization after experimental hemispherectomy: a structural and functional connectivity study

Willem M Otte[1,2], Kajo van der Marel[2], Maurits PA van Meer[2], Peter C van Rijen[3], Peter H Gosselaar[3], Kees PJ Braun[1,4] and Rick M Dijkhuizen[2,4]

Hemispherectomy is often followed by remarkable recovery of cognitive and motor functions. This reflects plastic capacities of the remaining hemisphere, involving large-scale structural and functional adaptations. Better understanding of these adaptations may (1) provide new insights in the neuronal configuration and rewiring that underlies sensorimotor outcome restoration, and (2) guide development of rehabilitation strategies to enhance recovery after hemispheric lesioning. We assessed brain structure and function in a hemispherectomy model. With MRI we mapped changes in white matter structural integrity and gray matter functional connectivity in eight hemispherectomized rats, compared with 12 controls. Behavioral testing involved sensorimotor performance scoring. Diffusion tensor imaging and resting-state functional magnetic resonance imaging were acquired 7 and 49 days post surgery. Hemispherectomy caused significant sensorimotor deficits that largely recovered within 2 weeks. During the recovery period, fractional anisotropy was maintained and white matter volume and axial diffusivity increased in the contralateral cerebral peduncle, suggestive of preserved or improved white matter integrity despite overall reduced white matter volume. This was accompanied by functional adaptations in the contralateral sensorimotor network. The observed white matter modifications and reorganization of functional network regions may provide handles for rehabilitation strategies improving functional recovery following large lesions.

Journal of Cerebral Blood Flow & Metabolism (2015) **35,** 1358–1367; doi:10.1038/jcbfm.2015.101; published online 13 May 2015

Keywords: brain plasticity; functional connectivity; graph analysis; hemispherectomy; rat brain; sensorimotor network

INTRODUCTION

Brain plasticity after hemispherectomy, the surgical disconnection, or removal of one cerebral hemisphere in patients with catastrophic epilepsy, illustrates the resilience of the brain to extensive lesions.

Many experimental and clinical studies provide strong evidence for widespread structural remodeling after extensive unilateral brain injury. There is also increasing support for the hypothesis that this remodeling underlies the remarkable cognitive and functional recovery after hemispherectomy (for recent reviews see ref. 1). A better understanding of the mechanisms underlying functional recovery after hemispherectomy may guide development of postoperative rehabilitation strategies that enhance these contralateral processes, which may also be relevant to injuries affecting large parts of a cerebral hemisphere, such as massive unilateral stroke. However, characterizing functional recovery and plasticity-related changes in hemispherectomized patients—or patients with large hemispheric lesions—is problematic. First, groups of patients are heterogeneous in terms of etiology, preoperative hemispheric damage and age at surgery, and brain plasticity and functional recovery are dependent on both. For instance, a recent study in children that underwent functional hemispherectomy found clear differences in motor outcome between children with congenital disorders as compared with those with acquired pathology.[2] Second, hemispherectomy is applied to patients who experienced severe epilepsy, which is known to significantly affect functional connectivity and structural integrity.

There are many important but unanswered questions regarding effects of hemispheric lesioning. For instance, it remains unclear how hemispherectomy—or extensive hemispheric damage—affects the remaining hemisphere; which structural adaptations occur; and how functional modifications are related to functional recovery. Ideally, these questions would be studied in a standardized and homogeneous experimental brain model that excludes aversive effect of previous (epileptogenic) lesions and concurrent (antiepileptic) drug therapy, with repetitive *in vivo* measurements that allow longitudinal assessment of whole-brain network changes in a non-invasive manner.

In this study, we aimed to characterize the relationship between cerebral reorganization and sensorimotor recovery in the

[1]Department of Pediatric Neurology, Rudolf Magnus Institute of Neuroscience, University Medical Center, Utrecht, The Netherlands; [2]Biomedical MR Imaging and Spectroscopy Group, Image Sciences Institute, University Medical Center, Utrecht, The Netherlands and [3]Department of Neurosurgery, Rudolf Magnus Institute of Neuroscience, University Medical Center Utrecht, Utrecht, The Netherlands. Correspondence: Dr WM Otte, Biomedical MR Imaging and Spectroscopy Group, Image Sciences Institute, University Medical Center, Utrecht, Yalelaan 2, Utrecht 3584 CM, The Netherlands.
E-mail: w.m.otte@umcutrecht.nl or wim@invivonmr.uu.nl
This work was supported by the Dutch National Epilepsy Fund [NEF 12.05], the Utrecht University's High Potential program, the Netherlands Organization for Scientific Research (NWO-VICI 016.130.662), and the Dutch Brain Foundation [F2014(1)-06].
[4]These authors contributed equally to this work.
Received 27 November 2014; accepted 10 April 2015; published online 13 May 2015

remaining hemisphere not impeded by congenital or acquired deficits, epilepsy, or pharmacological interventions. To that aim, we used an experimental anatomical hemispherectomy rat model and used non-invasive magnetic resonance imaging (MRI) and behavioral testing to map the spatiotemporal profiles of contralateral white matter integrity and functional connectivity in relation to changes in sensorimotor function. We specifically focused on the corticospinal tract as distinct changes in the integrity of this white matter structure have been found in children after hemispherectomy.[3,4] The choice of methods used for the *in vivo* assessment of the spatial and temporal pattern of functional changes in the contralateral hemisphere in the current study was based on previous experimental studies in an ischemic stroke rat model with similar large unilateral brain lesions and sensorimotor function changes[5] as observed after hemispherectomy.

MATERIALS AND METHODS

Animals

This study was carried out in strict accordance with the recommendations in guidelines of the European Communities Council Directive. The protocol was approved by the Utrecht University Ethical Committee on Animal Experiments (DEC 2008.I.09.065). ARRIVE guidelines were followed in the preparation of the manuscript. All efforts were made to minimize suffering. A total of 24, 9-week-old male Sprague-Dawley rats (Charles River Laboratories International, Wilmington, MA, USA), were included in the study. Twelve rats were assigned to anatomical hemispherectomy, and 12 rats served as age-matched controls. All animals were group-housed under standard, controlled conditions (food and water provided *ad libitum*, room temperature 22°C to 24°C, 12 hour light/12 hour dark cycle).

Hemispherectomy Model

Hemispherectomy in rats has been previously described in the studies by Machado and Marino *et al*,[6,7] on which we based our surgical procedure. Before anatomical hemispherectomy, rats were anesthetized with a subcutaneous injection of a mixture of 0.315 mg/mL fentanyl citrate and 10 mg/mL fluanisone (0.55 mL/kg, Hypnorm, VetaPharm, Leeds, UK) and 50 mg/mL midazolam (0.55 mL/kg, Dormicum, Roche Nederland B.V., Woerden, The Netherlands). During surgery the rat's body temperature was maintained with an in-house built heating pad. Before hemispherectomy, rats received an intramuscular injection of 5 mg/kg (10 mg/mL) gentamicin (Centrafarm, Etten-Leur, The Netherlands) to prevent infection.

A 2.5-cm long medial incision was made in the skin covering the skull and the pericranium. Right craniotomy was performed to expose the dura mater from 7 mm anterior to bregma back to the interaural line 9 mm posterior to bregma, including the temporal bone at –5 mm from bregma. Next, the middle cerebral artery was coagulated, followed by microsurgical resection of all neocortical tissue rostral to the tentorium, up to the bulbar area, white matter, hippocampus, and most parts of the basal ganglia, using a microsurgical suction apparatus connected to a vacuum pump (in-house built). A schematic representation of the microsurgically resected brain tissue is given in Supplementary Figure 1. In addition to the coagulation of the middle cerebral artery, we used antihemorrhagic absorbable gelatin sponge (Spongostan, Ferrosan Medical Devices A/S, Soeborg, Denmark) to minimize bleedings. After application of small pieces of gelatin sponge, the removed bone cap was replaced and the scalp was sutured. After surgery, animals were given 0.3 mg/mL subcutaneous buprenorphine analgesia (0.1 mL/kg, Temgesic, Schering-Plough Nederland B.V., Houten, The Netherlands) directly after surgery and 12 hours later. During the first 2 days, rats were housed individually. Daily weight loss was monitored and weight loss over 10 g per 24 hours was compensated for by subcutaneous injection of 5–15 mL Ringer's lactate (Baxter, Utrecht, The Netherlands).

Sensorimotor Function Testing

Functional behavioral testing involved calculation of a composite SPS, which has been effectively used to assess loss and recovery of sensorimotor function after unilateral cerebral ischemic injury in rats. The method is described in detail in the study by van der Zijden.[8] In brief, six different motor, sensory, and tactile tests were applied, scoring motility and spontaneous activity, gait disturbances, postural signs, and limb placing. Scoring was done before each MRI session and at intermediate time points, namely on day 1, 3, 14, 21, and 35 post surgery. This provided an overall SPS on a scale of 0 to –20 points, with –20 representing maximum deficit.

MRI Acquisition

Functional and structural MRI data was acquired at 7 and 49 days after hemispherectomy. The first time point allowed MRI at a subacute stage when animals had recovered from surgery. The second time point was based on previous sensorimotor studies in a rat model of unilateral ischemic stroke that found significant recovery of functional outcome within 7 weeks.[9] Rats were anaesthetized with 4% isoflurane for endotracheal intubation, followed by mechanical ventilation (rate: 52–59/min; Columbus Instrument, Columbus, OH, USA) with 2.0% isoflurane in air/O_2 (2:1) during MRI acquisition.

Magnetic resonance imaging measurements were conducted on a 4.7 T horizontal bore MR system (Varian, Palo Alto, CA, USA) with a gradient-coil insert (125 mm internal diameter; 500 mT/m maximum gradient strength with 110 μs rise time) (Magnex Scientific, Oxford, UK). A Helmholtz volume coil (90 mm diameter) and an inductively coupled surface coil (25 mm diameter) were used for signal excitation and detection, respectively. Rats were placed in an MR-compatible stereotactic holder, and immobilized with earplugs and a tooth-holder. During MRI, blood oxygen saturation and heart rate were continuously monitored by a pulse oximeter (8,600 V, Nonin Medical, Plymouth, MN, USA) with the probe positioned on a hindpaw. In addition, expired CO_2 was continuously monitored with a capnograph (Multinex 4200, Datascope, Fairfield, NJ, USA), and body temperature was maintained at 37.0°C ± 0.5°C using a feedback-controlled heating pad. End-tidal CO_2 levels were kept within the normal range, equivalent to arterial pCO_2 levels between 35 and 45 mm Hg (calculated from previous calibration measurements), by adjusting ventilation volume and/or rate.

Structural MRI. The structural MRI acquisitions included multi-slice T_2-weighted spin-echo MRI at 12 different echo times (repetition time (TR)/echo time (TE) = 3,600/15 – 180 ms (15 ms intervals); 19 1-mm coronal slices; field-of-view = 32 × 32 mm^2; acquisition matrix = 256 × 128; voxel resolution = 0.125 × 0.25 × 1.0 mm^3) and diffusion tensor imaging (DTI) (four-shot spin-echo EPI; TR/TE = 3,500/26 ms; 25 0.5-mm transversal slices; field-of-view = 32 × 32 mm^2; acquisition matrix = 64 × 64; voxel resolution = 0.5 × 0.5 × 0.5 mm^3; diffusion-weighting in 50 directions with b = 1,250 s/mm^2 (Δ/δ = 11/6 ms); 2 images without diffusion-weighting (b = 0 s/mm^2)).

Functional MRI. Repetitive blood oxygenation level-dependent (BOLD) resting-statestate functional MRI (rs-fMRI) was conducted using a gradient echo single shot EPI sequence (TR/TE = 500/19 ms; 7 1.5-mm coronal slices; field-of-view = 32 × 32 mm^2; acquisition matrix = 64 × 64; voxel resolution, 0.5 × 0.5 × 1.5 mm^3; pulse angle = 35°; temporal resolution = 500 ms; number of scans = 1,200; total scan time = 10 min). Exactly 10 minutes before rs-fMRI acquisition, end-tidal isoflurane anesthesia concentration was reduced to 1.0%, which was maintained during rs-fMRI.

At this level of isoflurane anesthesia, cerebral glucose utilization, cerebral blood flow coupling, and functional connectivity, including the long distance connections, are largely preserved.

Image Processing

Image registrations were performed with ELASTIX (http://elastix.isi.uu.nl). In short, the registrations were based on multi-resolution schemes with 'mutual information' as the similarity measure. The optimization method used was a gradient descent, and interpolation methods were spline interpolation for images and nearest neighbor interpolation for regions-of-interest (ROIs).

Absolute T_2 values were calculated using nonlinear Levenberg–Marquardt fitting of the multi-echo T_2-weighted signal intensities. Absolute T_2 maps were used to manually delineate the areas of ipsilaterally removed tissue at day 7. After bias-field inhomogeneity correction and removal of signal from non-brain structures, the first echo image of the multi-echo T_2-weighted scans was non-linearly registered to an anatomical reference image that was matched to a three-dimensional model of the Paxinos and Watson stereotactic rat brain atlas (4th edition). This corrected for moderate deformations such as midline shift after hemispherectomy.

Structural Image Analysis—White Matter

Diffusion-weighted images were corrected for motion and residual eddy current distortion. The effective diffusion tensor, the corresponding eigensystem, and the subsequently derived fractional anisotropy (FA), mean diffusivity (MD), axial diffusivity, and radial diffusivity (RD) were computed for each voxel.

Separate nonlinear registration was performed to match individual subjects' FA images with an average rat brain FA template. These registrations allowed us to project the cerebral peduncle white matter template region in individual subject space, both ipsi and contralaterally to calculate the volume of the cerebral peduncle and its average DTI-derived parameters. The cerebral peduncle was selected as critical white matter region, since it includes the pyramidal tracts (corticospinal and corticonuclear tracts).

To obtain a general indication of changes in contralateral white matter after hemispherectomy, we measured total white matter volume in the remaining hemisphere. To estimate hemispheric white matter volumes, we applied a multiparametric meta-classifier to all voxels in the contralateral hemisphere in the control and hemispherectomy groups. This meta-classifier (based on the random forest algorithm[10]) allows straightforward and unbiased white matter segmentation in rat brain. For each voxel in the contralateral hemisphere, the white matter probability is calculated based on FA, MD, and T_2 intensities, as well as spatial features.[11] Total and relative volumes (that is, relative to the total contralateral hemispheric volume) were calculated from individual voxel probabilities.

Functional Image Analysis—Gray matter

Functional images were linearly registered with the first echo image of the T_2-weighted scans (which was aligned with the rat brain atlas). We masked out the ipsilateral hemisphere because of hypointense areas in the post-surgical cavity that disturbed the registration process. Matching of the atlas and the functional data allowed the projection of cortical and subcortical ROIs on the functional images.

Functional connectivity was calculated from rs-fMRI data at a ROI level. To that aim, we projected the primary motor cortex (M1), caudate-putamen complex (CPu), and primary somatosensory forelimb area (S1FL) from rat brain atlas to subject space. The selection of these three regions out of a larger list of sensorimotor areas was based on previous experimental stroke work that found large modifications in these regions.[9]

Non-neuronal signal contributions were minimized by means of spatial smoothing (Gaussian kernel with 1.0 mm full width at half maximum), band-pass filtering (0.01–0.1 Hz) and linear regression with nuisance signals, including the mean brain BOLD activity. To understand the spatial changes in functional connectivity in the contralateral hemisphere at large, we obtained connectivity (using the Pearson's correlation coefficient *r*) maps by correlating the average ROI signal, for all three ROIs separately, with all brain voxels. Interregional functional connectivity between the M1 and other ROIs was determined as *r* between the mean low-frequency BOLD signal fluctuations in pairs of ROIs. For all three ROIs, intraregional signal coherence was calculated as the mean *r* between the low-frequency BOLD signal fluctuations of each voxel within each ROI and the average low-frequency BOLD signal time series of that ROI.

Functional Network Analysis

Besides connectivity patterns in the M1, CPu, and S1FL, we also evaluated functional connectivity at a network level using graph analysis, an elegant tool to assess whole-brain connectivity from a network representation.[12] Complex relational states between remote brain regions within network representation can be measured from the average shortest path length and the overall clustering coefficient.

From the Paxinos and Watson rat brain atlas, we carefully selected 15 left-sided (i.e., from the intact hemisphere) sensorimotor network regions, large enough to contain multiple voxels at the applied fMRI resolution. The anatomical regions and their atlas abbreviation are listed in Supplementary Table 1.

For every individual animal at each time point, we constructed a 15×15 weighted undirected network and determined average shortest path length and overall clustering coefficient. Details are available as Supplementary Information.

Statistical Analysis

The change in SPS in the hemispherectomy group (given as count data) was examined using linear Poisson regression with time point as factor and scores at day 1 as reference.

The following data were analyzed using linear mixed modeling (R package nlme: http://cran.r-project.org/web/packages/nlme/): (i) absolute and relative white matter volumes, (ii) volume, FA, MD, axial diffusivity, and RD values within the ipsi and contralateral cerebral peduncle, (ii) interregional functional connectivities, (iii) intraregional signal coherences, and (iv) shortest path length and clustering coefficient values within the functional network. Linear mixed modeling has recently been suggested to be used in the analysis of longitudinal MRI data as it offers superior statistical power in detecting serial group differences.[13]

Except for shortest path lengths and clustering coefficients, the linear mixed models included the factors group (i.e., control or hemispherectomy) and time (i.e., day 7 or 49). We added a random intercept per subject. We did not include a group × time interaction as this decreased the likelihood of the models. Potential temporal correlations within rats were corrected with an autocorrelation structure of order 1, with a continuous time covariate. Group differences at individual time points were *post-hoc* tested using an independent Student's *t*-test.

The functional network linear mixed models included an additional level of nesting, namely, network nodes (i.e., nodes within subjects within time). These models were specified with the following fixed factors: group × node interaction and time × node interaction. Correlations within and between subjects were corrected with random intercepts for nodes nested within subjects, and an additional unstructured correlation matrix with nodes nested within subjects.

We considered $P < 0.05$ as significant. All values are presented as mean ± s.d.

RESULTS

Anatomical Hemispherectomy

Hemispherectomy was successful in 8 of 12 rats. The ipsilateral neocortex, white matter (e.g., corpus callosum and capsula externa), hippocampus, and substantial part of the basal ganglia, including the caudate-putamen complex were resected with preservation of the diencephalon. The removal of subcortical regions was not identical in all rats owing to limitations in hemostasis. Bleedings from penetrating arteries and the anterior cerebral artery (coagulation was not possible owing to close vicinity of the sagittal sinus vein) could not be adequately controlled in all animals. This variability in subcortical tissue removal is reflected in the MRI-based lesion incidence map that displays the percentage of animals with removed tissue on a voxel-by-voxel basis in the brain at 7 days post surgery (Figure 1A). Nevertheless, decortication was highly reproducible.

Animals developed hemiparesis from which they largely recovered within a week (see below). Body weight dropped during the first 2 weeks post surgery, owing to disrupted food intake (despite Ringer's lactate injections), but returned to control levels in the weeks thereafter. Two rats showed aggressive behavior toward cage mates in the first week after surgery, and were kept individually until the second week.

The four animals in which hemispherectomy was unsuccessful died from post-surgical intracranial hemorrhage within 24 hours ($n = 3$) or developed post-surgical hydrocephalus ($n = 1$; terminated after the 7 days of MRI scan). These were excluded from further analysis.

Recovery After Initial Sensorimotor Deficiency

Sensorimotor function, measured from the SPS, was notably reduced after hemispherectomy (Figure 1B). Motility was severely disturbed during the first week after surgery with rats moving only in response to stimuli. Motility recovered to levels of normal or slightly reduced exploratory behavior in the days thereafter. The SPS at 3, 7, 14, 35, and 49 days was significantly higher as compared with day 1 post hemispherectomy. The SPS score at 49 days was significantly higher as compared with the SPS at days 1, 3, and 7. Gait disturbances were found in all animals

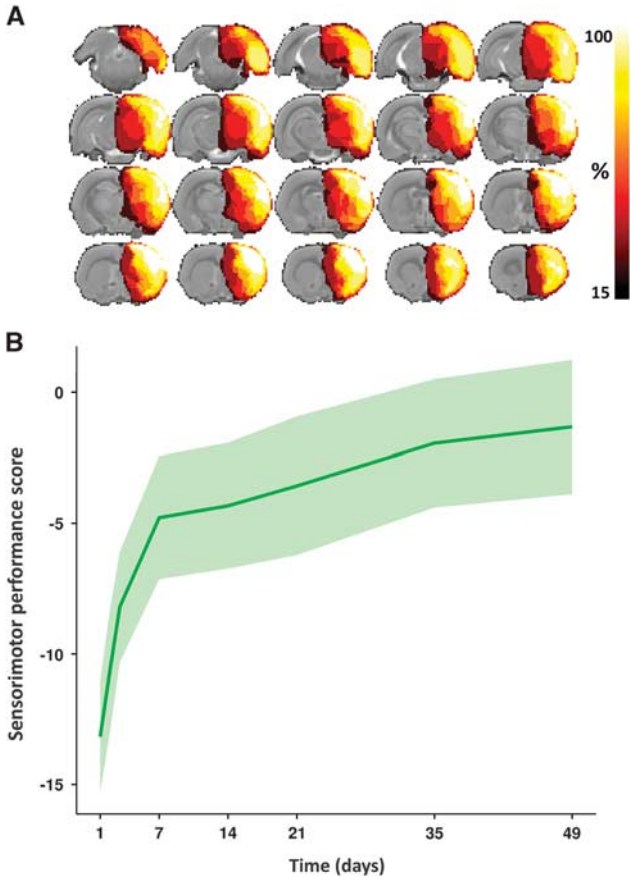

Figure 1. Removed brain tissue incidence map and sensorimotor performance. (**A**) Map of the removed tissue incidence after right-sided anatomical hemispherectomy in eight rats, as determined on T_2-weighted structural scans. The lesion incidence maps are overlaid on consecutive coronal slices from a multi-slice T_2-weighted anatomical rat brain template. The voxel intensities represent the percentage of animals that displayed tissue loss at that specific location at 7 days post surgery. In all animals, ipsilateral cortical tissue was successfully removed. Furthermore, additional removal of (parts of) the CPu and hippocampus was attained in the majority of animals. (**B**) Sensorimotor performance score as a function of time after hemispherectomy (median (line) ± interquartile range (shaded area)). CPu, caudate-putamen complex.

with constant circling toward the paretic side in the first days after hemispherectomy, and alternate circling and walking toward the paretic side at later stages. Concomitant deficits included weak or no placing of ipsilateral and contralateral forelimbs, and limited degree of limb flexion, body rotation, and resistance against lateral push. Remaining deficits up to 49 days after surgery were predominantly owing to incomplete restoration of limb flexion, body rotation, and forelimb placement.

Degeneration of Ipsilateral and Preservation of Contralateral Cerebral Peduncle

Microstructural white matter tract integrity was assessed with DTI. We focused on the cerebral peduncle, which includes the pyramidal tracts that connect cortical areas to the spinal cord (corticospinal tract) and brain stem (corticonuclear tract). On visual inspection of the DTI-derived FA maps, the bilateral cerebral peduncles appeared symmetrical in fiber direction and anisotropy in the control animals, whereas the ipsilateral cerebral peduncle was mostly unidentifiable after hemispherectomy (Figure 2).

We observed no significant FA changes in the tissue bordering the resection area at 49 days.

At a group level, the ipsilateral cerebral peduncle was significantly reduced in volume after hemispherectomy (group effect $-0.68 \pm 0.09\,mm^3$; $P < 0.0001$). Furthermore, remaining ipsilateral cerebral peduncle tissue was characterized by a significantly decreased FA in the hemispherectomy group (group effect -0.29 ± 0.02, $P < 0.0001$; no time effect). Additional differences between the control and hemispherectomy groups were present for MD ($0.08 \pm 0.03 \times 10^{-3}\,mm^2/s$, $P = 0.03$), axial diffusivity ($-0.31 \pm 0.04 \times 10^{-3}\,mm^2/s$, $P < 0.0001$), and RD ($0.27 \pm 0.03 \times 10^{-3}\,mm^2/s$, $P < 0.0001$). Time effects were found for mean, axial, and RD (MD: $0.004 \pm 0.001 \times 10^{-3}\,mm^2/s$, $P = 0.004$; axial diffusivity: $0.004 \pm 0.001 \times 10^{-3}\,mm^2/s$, $P = 0.003$; and RD: $0.004 \pm 0.001 \times 10^{-3}\,mm^2/s$, $P = 0.01$), owing to a change over time in the hemispherectomy group.

The contralateral cerebral peduncle volume increased over time in the hemispherectomy group ($0.44 \pm 0.13\,mm^3$; $P < 0.004$). The FA of the contralateral peduncle increased over time in the hemispherectomy animals (0.0008 ± 0.0003; $P = 0.006$). A group difference was also measured for FA in the contralateral peduncle (-0.03 ± 0.01; $P = 0.0017$). In addition, we found group effects for the MD ($0.03 \pm 0.01 \times 10^{-3}\,mm^2/s$, $P = 0.04$) and RD ($0.048 \pm 0.015 \times 10^{-3}\,mm^2/s$, $P = 0.004$). Axial diffusivity increased over time in the hemispherectomy ($0.002 \pm 0.0004 \times 10^{-3}\,mm^2/s$; $P < 0.0001$).

Reduction of Contralateral Hemispheric White Matter Volume

Results from measurements of the total absolute and relative white matter volume in the contralateral hemisphere are shown in Figure 3. Significant group and time effects were found for the absolute contralateral white matter volume. Contralateral hemispheric white matter volume increased in controls from 93.0 ± 3.0 to $111.0 \pm 2.28\,mm^3$ 6 weeks later ($P < 0.0001$; Figure 3A). Contralateral white matter volume in hemispherectomized rats was not significantly different from controls, at the acute time point. At the chronic time point, contralateral white matter volume in hemispherectomized rats was significantly lower as compared with controls of the same age ($-14.0 \pm 4.8\,mm^3$; $P = 0.01$).

Identical patterns were found if contralateral white matter volume was expressed as relative to the total hemispheric volume. At the chronic time point, relative white matter volume was significantly lower in hemispherectomized rats as compared with controls ($-1.33 \pm 0.32\%$, $P = 0.001$).

Increased Functional Connectivity of Contralateral Sensorimotor Areas

Resting state functional magnetic resonance imaging allowed measurement of spontaneous low-frequency BOLD fluctuations, which enabled the assessment of changes in signal synchronization within and between brain regions after hemispherectomy. We focused on functional connectivity in and between sensorimotor areas in the intact hemisphere.

Seed-based mean functional connectivity maps of the contralateral M1, CPu, and S1FL clearly demonstrated distinct intrahemispheric functional connectivity enhancement in the remaining hemisphere after hemispherectomy as compared with control animals. This was more pronounced at 7 days than at 49 days post hemispherectomy (Figure 4). The control group showed strong and consistent interhemispheric functional connectivity between homotopic bilateral M1, CPu, and S1FL areas at both time points.

In the remaining hemisphere in the hemispherectomy group, M1 exhibited higher connectivity with CPu and S1FL, which was most pronounced at 7 days after hemispherectomy. Negative correlations between M1 and the thalamus were observed at day 49. CPu's intrahemispheric functional connectivity was elevated at day 7, particularly with primary and secondary somatosensory,

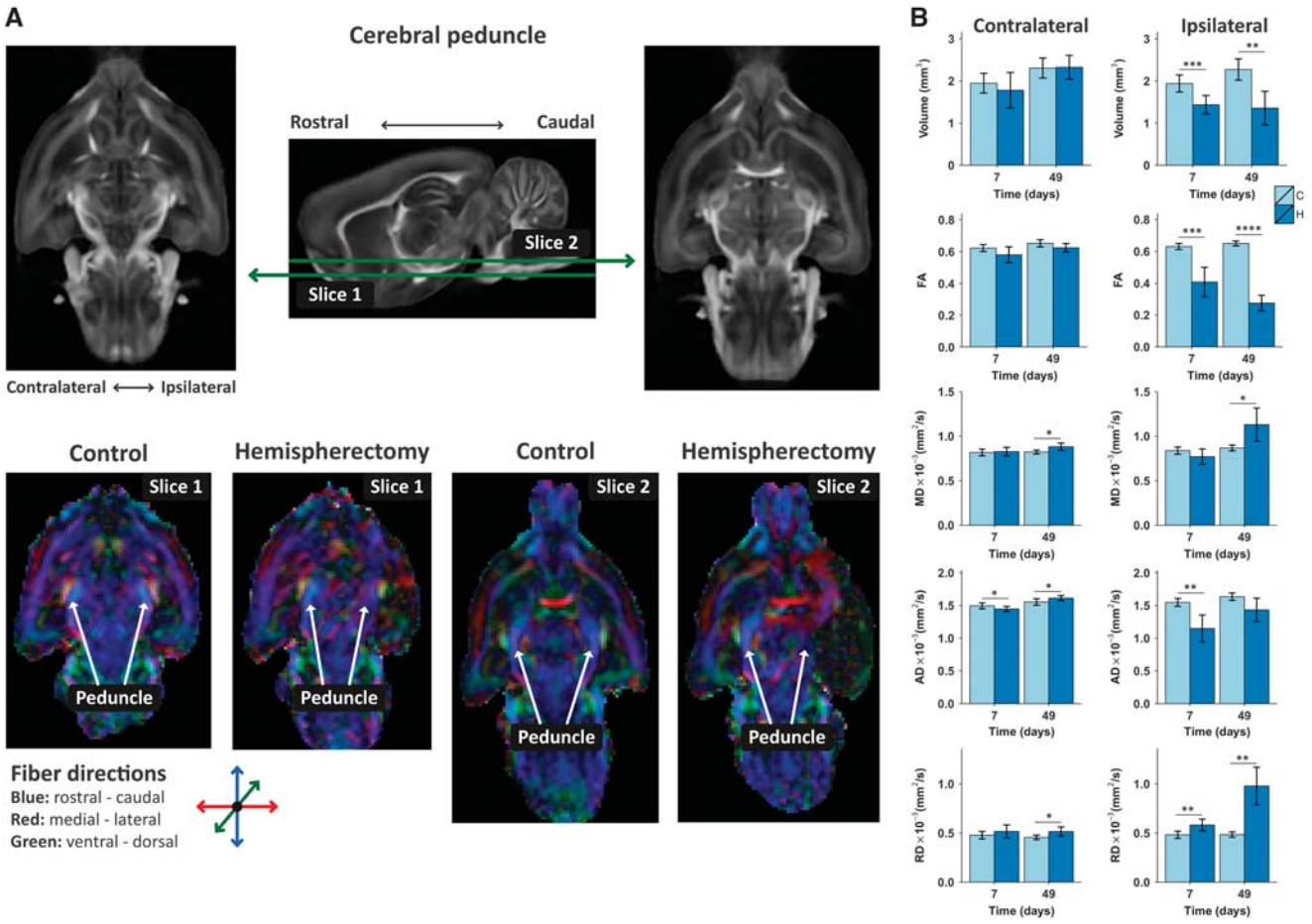

Figure 2. Ipsi and contralateral cerebral peduncle integrity after hemispherectomy. (**A**) Examples of diffusion tensor imaging-derived fractional anisotropy (FA) maps of rat brains at 49 days after hemispherectomy and of age-matched controls. Two transversal slices, including the cerebral peduncle, are shown at different ventral–dorsal levels as depicted on the sagittal FA rat brain template image (middle). The cerebral peduncle, running predominantly in rostral–caudal direction displayed symmetrical fiber orientation and FA values in control rat brain (C) ipsi and contralaterally (bottom; slice 1 and slice 2). The FA in the contralateral cerebral peduncle of hemispherectomized rat brain (H) was similar to that in control rat brains, but ipsilaterally it displayed irregular fiber orientation and low FA. (**B**) Cerebral peduncle regions-of-interest-based volume, FA, mean diffusivity (MD), axial diffusivity (AD) and radial diffusivity (RD), contralaterally and ipsilaterally at days 7 and 49. Bars represent group mean ± s.d.; *$P < 0.05$; **$P < 0.01$; ***$P < 0.001$; ****$P < 0.0001$ versus controls as revealed by *post-hoc* analysis.

and motor cortices, which normalized at 49 days after hemispherectomy. There were strong negative signal correlations between CPu and the thalamic area 49 days after hemispherectomy. Functional connectivity of S1FL with the CPu was increased at 7 days after hemispherectomy, which decreased thereafter.

For statistical comparison, we calculated the average functional connectivity within M1, S1FL, and CPu (Figure 5A). In the contralateral M1, the intraregional signal coherence increased over time in both experimental groups (0.06 ± 0.02; $P = 0.04$). No group effect was found in M1. A significant group effect was present for intraregional signal coherence in S1FL, which was elevated in the hemispherectomy group (0.13 ± 0.05; $P = 0.03$). No group difference in intraregional signal coherence was found in the contralateral CPu.

Functional connectivity between contralateral M1 and contralateral CPu, and S1FL are shown in Figure 5B. Interregional functional connectivities were significantly elevated between M1 and CPu (average group effect: 0.23 ± 0.09; $P = 0.02$), and between M1 and S1FL (group effect: 0.32 ± 0.09, $P = 0.003$).

Remodeled Contralateral Sensorimotor Network

Functional connectivity was also measured at a network level using graph analysis. The spatial location of the sensorimotor network nodes is shown in Figures 6A and 6B. An example of a weighted functional connectivity matrix is shown in Figure 6D. The average shortest path lengths and average clustering coefficients for the contralateral sensorimotor network are plotted in Figure 6C. We found no significant node × group effect for shortest path length, but a significant node × time effect was present ($P = 0.0003$), indicating no overall group differences but a change over time. The node × group and node × time interactions were significant for the clustering coefficient ($P = 0.04$ and $P < 0.0001$, respectively), indicating an overall difference between groups and over time. As much information was lost by averaging values over all network nodes, we also plotted the individual network node's shortest path lengths and clustering coefficients as shown in Figure 7. Since *post-hoc* testing of individual time points within nodes may inflate the false positive rate, we only report the multilevel mixed-model effects in the figure. Significant time effects for the shortest path length were found for S1FL,

S1BF, S1HL, S1J, S1, S1ULp, and S2. A group effect was found for the S1ULp node, indicating a lower shortest path length to all other network nodes after hemispherectomy. A significant clustering coefficient time effect was found for M1, M2, CPu, thalamus, S1BF, S1Sh, and external globus pallidus. A group difference in clustering coefficient was present for the M2, thalamus, S1J, and Cg nodes, with higher clustering in the hemispherectomy group as compared with controls (Figure 7).

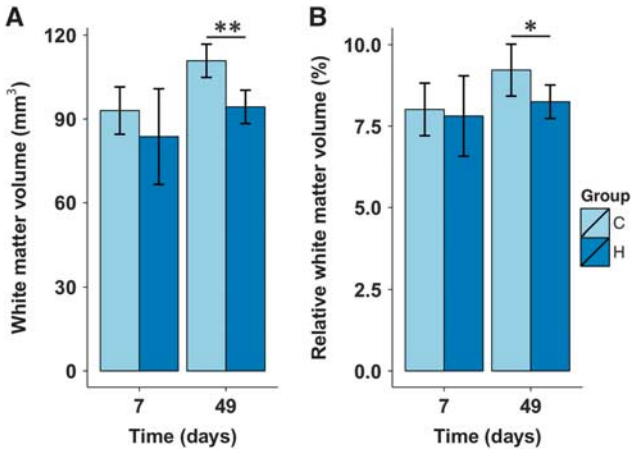

Figure 3. Absolute and relative contralateral white matter volumes. (**A**) Absolute contralateral white matter volume at day 7 and 49 in control (C) and hemispherectomized (H) rats. (**B**) Contralateral white matter volume relative to total contralateral hemispheric volume (this corrects for total brain volume as a potential confounder for white matter volume differences between control and hemispherectomized rats). Bars represent group mean ± s.d.; $^{*}P < 0.05$; $^{**}P < 0.01$ versus controls as revealed by *post-hoc* analysis.

DISCUSSION

Hemispherectomy caused considerable sensorimotor deficits in young adult rats, which was followed by significant recovery within 2 weeks. Important cerebral changes during this recovery included (i) increased axial diffusivity in the contralateral cerebral peduncle, (ii) enhanced inter and intraregional functional connectivity in the contralateral hemisphere, and (iii) stronger degree of functional clustering in the contralateral sensorimotor network, particularly involving the motor cortex and thalamus.

The spontaneous functional recovery reflects the plastic capacities of the brain, i.e., structural and functional adaptation of neuronal configuration and rewiring that underlies the restoration of sensorimotor outcome.[14–16] Earlier behavioral and preclinical studies on neural reorganization and functional recovery after hemispherectomy have been mostly conducted in nonhuman primates.[17] Our study demonstrates that a rodent hemispherectomy model provides a useful means to assess certain aspects of (intrinsic) restorative processes. Furthermore, our advanced MRI protocol allowed longitudinal *in vivo* assessment of multiple structural and functional measures of brain integrity together with changes in behavioral status over time.

The rate and extent of sensorimotor recovery after hemispherectomy are known to be age dependent. Previous preclinical hemispherectomy studies have described that young hemispherectomized monkeys generally regain lower limb function within a year, although the upper limb remains hemiparetic.[17,18] Adult-lesioned vervet monkeys, displaying similar upper limb movement impairments as infant-lesioned monkeys, however, had enduring lower limb disturbance.[19] In our rat model, we found remarkable recovery of sensorimotor function in young adult hemispherectomized rats. This could suggest that the (young) adult rat brain is better capable to restore cerebral functions after hemispherectomy than the adult monkey brain. Our results cannot be extrapolated to other species without

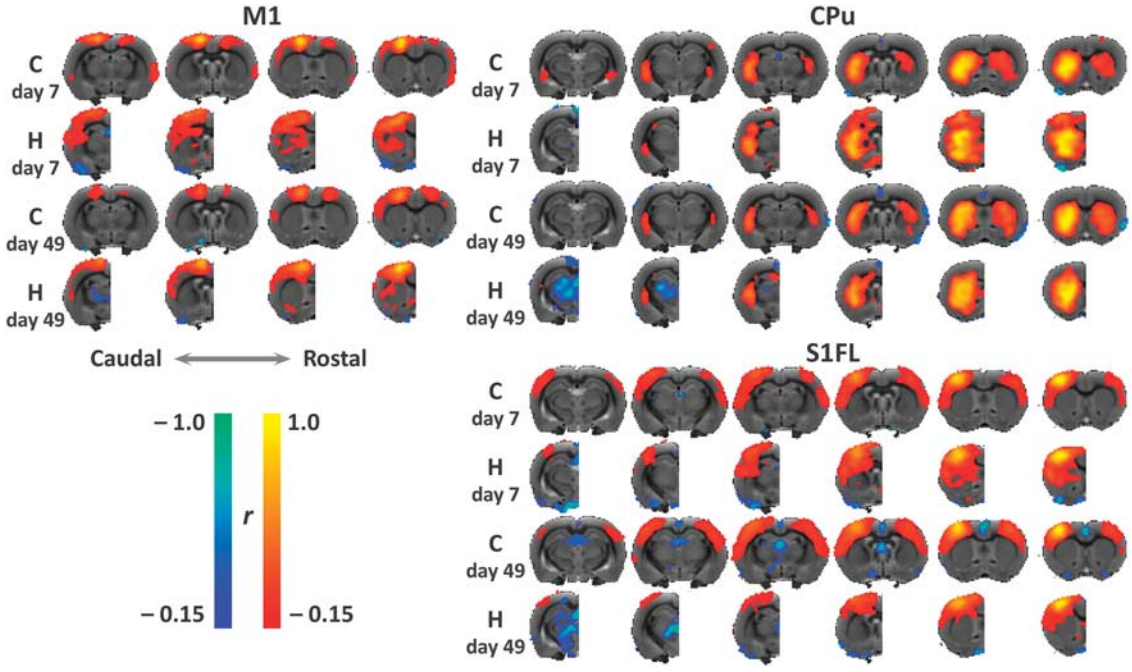

Figure 4. Spatial functional connectivity maps for the contralateral sensorimotor areas. Group mean functional connectivity maps, by correlation analysis of resting-state fMRI data, of the contralateral primary motor area (M1), caudate-putamen complex (CPu), and primary somatosensory forelimb area (S1FL) with the rest of the brain and overlaid on consecutive coronal slices from a multi-slice T_2-weighted anatomical rat brain template. Maps are shown for the control (C) and hemispherectomy (H) group at two time points (7 and 49 days after surgery). Positive and negative functional connectivity (*r*) values range from 0.15 to 1.0 and from –0.15 to 1.0, respectively.

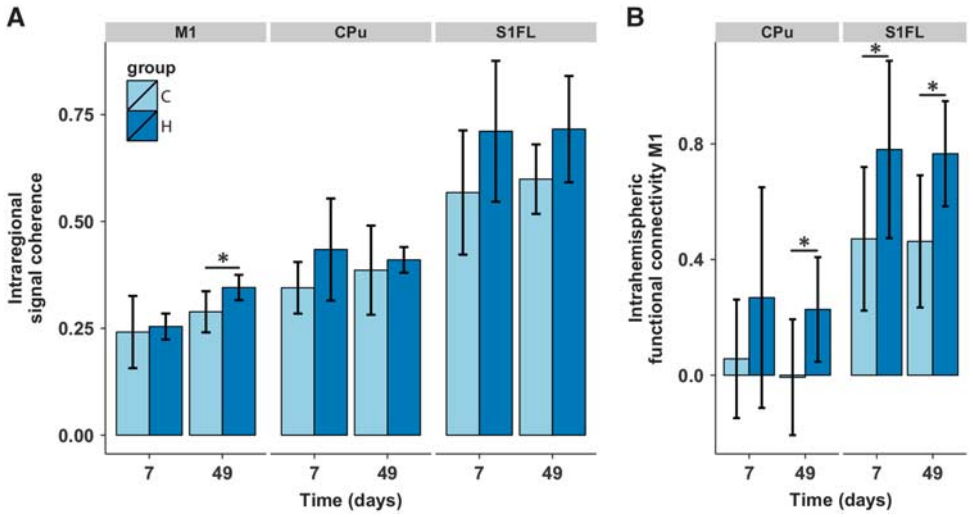

Figure 5. Intraregional signal coherence and interregional functional connectivity in the contralateral hemisphere. (**A**) Intraregional signal coherence of contralateral primary motor cortex (M1), caudate-putamen complex (CPu), and the primary somatosensory cortical forelimb area (S1FL). (**B**) Intrahemispheric functional connectivity of M1 with CPu and S1FL. Bars represent mean ± s.d. for the control (C) and hemispherectomy (H) groups at days 7 and 49. *$P < 0.05$ versus controls as revealed by *post-hoc* analysis.

caution, and additional studies are needed for reliable interspecies comparison.

Substantial recovery in rats has previously been demonstrated. An earlier study assessed the role of the remaining hemisphere in functional recovery after hemispherectomy in rats using motor area mapping.[6] Two weeks post hemispherectomy four out of seven rats showed bilateral body movements in response to stimulation of the remaining hemisphere, suggesting a latent capacity in the motor cortex to control bilateral motor function.

White matter growth in healthy rats was expected as continued fiber expansion and myelination, which is known to occur in healthy rats up to old age.[20,21] With this is mind, hemispherectomy significantly affected the integrity of the ipsi and contralateral cerebral peduncle. The ipsilateral cerebral peduncle largely disappeared, probably owing to Wallarian degeneration reflected by large reductions in FA and axial diffusivity as calculated from the DTI scans. Specifically, a reduction in axial diffusivity has been linked to axonal degeneration.[22] However, alternative biological processes, which may occur around white matter fibers after lesioning, could also have influenced our DTI-based measures. These include inflammation-associated vasogenic edema and cellularity around the fibers, leading to increased or decreased apparent diffusion coefficients, respectively.[23] In future studies, alternative techniques such as diffusion basis spectrum imaging may allow disentanglement of axonal injury, demyelination, and inflammation in a single MRI experiment.[24,25]

In contrast to previous studies after neonatal or adult stroke,[26–28] we observed no clear signs of increased FA in the tissue bordering the resection area at 49 days post hemispherectomy. This may be explained by our relatively large voxel size (0.125 mm^3), which might have blurred possible local FA changes in the perilesional tissue, or perilesional tissue may react differently if adjacent tissue is surgically removed rather than infarcted.

Two clinical studies that applied DTI to characterize reorganizational changes in the corticospinal tract and medial lemniscus after functional hemispherectomy have reported similar ipsilateral white matter changes.[3,4] Wakamoto *et al*[4] found degeneration of the ipsilateral corticospinal tract in children after functional hemispherectomy. There was, however, no evidence of reinforcement in the contralateral cerebral peduncle. Choi *et al*[3] reported an asymmetry in bilateral brainstem corticospinal tracts with preserved symmetry in the bilateral medial lemnisci.

Hemispheric lesions, comparable in size as measured in our study, are typical for the severe neonatal hypoxic-ischemic encephalopathy rat model (in 7- day-old rat with brain maturity equivalent to that of an early third trimester human fetus).[29] Hypoxia-ischemia-lesioned rats have been assessed with DTI at 1 year of age with a focus on white matter in general[26] and with respect to the visual system connections.[30] In these rats with developmentally early lesions—which include the visual cortex—both the retinocollicular and retrinogeniculate fiber bundles, projecting from the contralesional eye, are not degenerated and even display enhanced anterograde manganese transportation as compared with the opposite white matter bundles. Comparing data from the hemispherectomy model data with data from this early 7- day hypoxia-ischemia model, however, is complicated by distinct developmental and functional differences and specific post-lesion adaptations in young adult and neonatal brains.

Our rs-fMRI data revealed distinct functional connectivity changes in the remaining hemisphere after hemispherectomy. In particular, neuronal signal synchronization was significantly enhanced within the intact contralateral sensorimotor network. Enhancement of functional connectivity as early as 7 days after hemispherectomy may be related to early plasticity mechanisms in the remaining hemisphere. This could involve unmasking or recruitment of pathways that are normally suppressed by transcallosal inhibition, possibly in combination with reconfiguration of synaptic activity. Other neuronal plasticity mechanisms—which have also been associated with subacute recovery after stroke—may include spine elongation, neurite growth followed by synaptogenesis in the neocortex, rhythmic synchronized neuronal activity, and a state of extensive hyperexcitability. Whether these neuronal plasticity mechanisms underlie the changes reported in this study remains speculative and need further investigation using additional measurements at a cellular level, including assessment of potential involvement of glial, endothelial, and inflammatory processes.

Our findings show similarities but also differences with rs-fMRI-based data from our previous studies in a rat model for unilateral ischemic stroke.[9,31,32] In these studies, post-stroke sensorimotor recovery was particularly associated with restoration of functional connectivity between the intact ipsi and contralateral

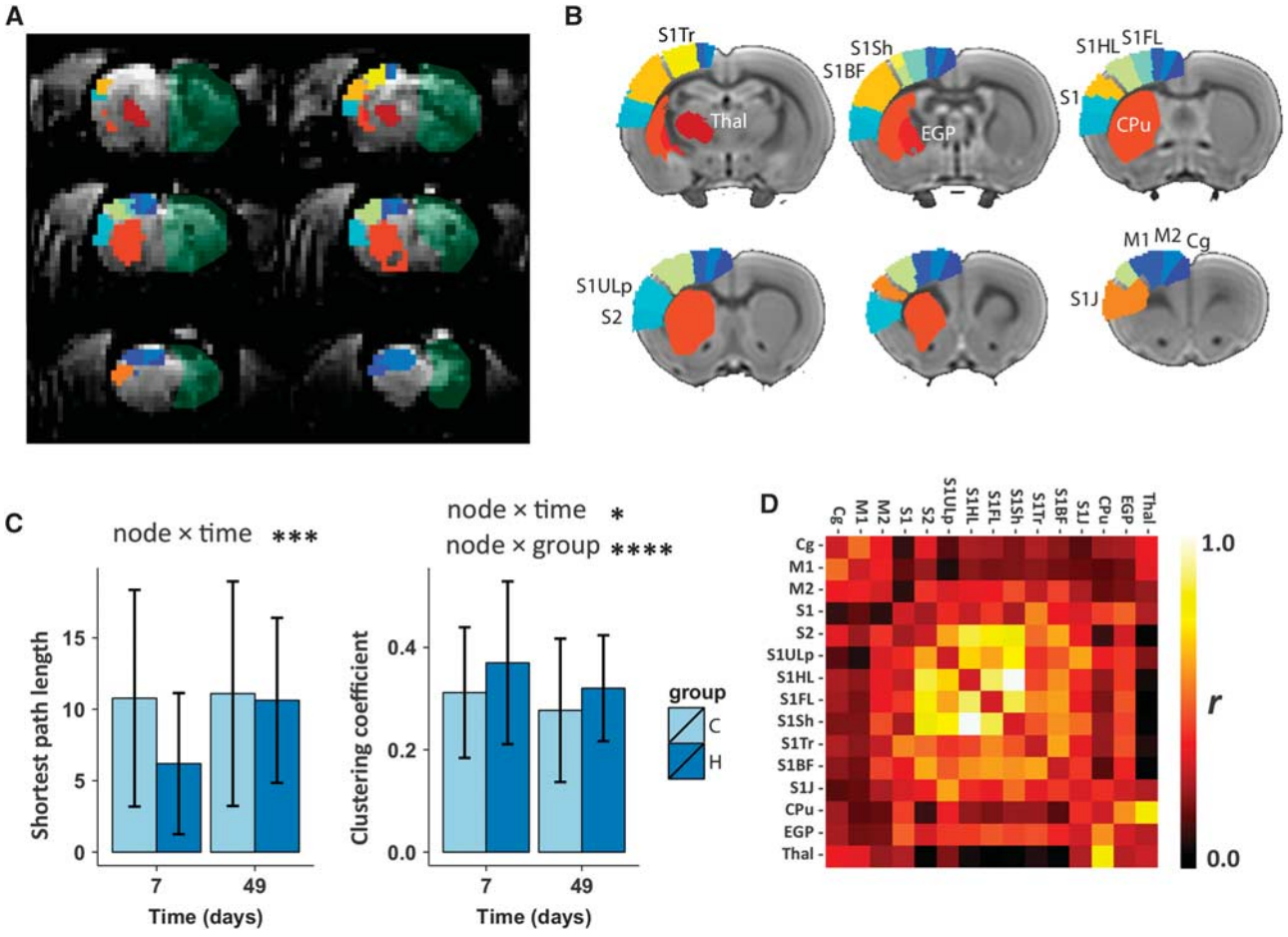

Figure 6. Contralateral sensorimotor network features. (**A**) From the Paxinos and Watson rat brain atlas, 15 cortical and subcortical sensorimotor regions were selected and projected on coronal slices of a representative resting-state BOLD image (not processed) from 1 of the animals at day 47. The removed hemisphere is marked as a semi-transparent green area. (**B**) The same sensorimotor regions, with identical color coding, are also projected on coronal slices of the left (contralateral) hemisphere of the rat brain template used for registration (one color per region and summarized in Supplementary Table 1). Each region represents a single network node in the weighted graph analysis. (**C**) Weighted shortest path length (left) and weighted clustering coefficient (right), averaged over all network nodes at two time points (7 and 49 days) in the control (C) and hemispherectomy (H) group. Statistical node × group and node × time output from the nested multilevel analysis are shown for significant nodes only. Bars represent group mean ± s.d.; $*P < 0.05$; $***P < 0.001$; $****P < 0.0001$ versus controls. (**D**) Example of Pearson's correlation (*r*) matrix for the 15 sensorimotor network nodes. The rows and columns represent individual nodes and their corresponding functional connectivity. BOLD, blood oxygenation level dependent; Cpu, caudate-putamen complex; M1, primary motor cortex; S1FL, primary somatosensory cortical forelimb area.

sensorimotor cortices. In addition, in line with our current data, progressively increasing intraregional signal coherence in contralateral sensorimotor regions, as well as enhanced intrahemispheric functional connectivity between contralateral sensorimotor regions, was found in animals with large unilateral ischemic lesions.[32] Intriguingly, recovery of the SPS after hemispherectomy in the present study was comparable to that observed in rats (of similar age) recovering from unilateral stroke despite the lack of structural (and consequently functional) interhemispheric connections between the bilateral sensorimotor cortices. This suggests that interhemispheric functional connectivity, although associated with post-stroke functional recovery, may not be critical for restoration of sensorimotor function. The enhancement of intraregional signal coherence in the contralateral sensorimotor areas, as observed in this study, may equally contribute to functional recovery, but this remains to be tested.

The negative correlation of signals from the thalamus with signals from the other areas at 7 weeks is in agreement with negative correlation of thalamic signals within the motor network that has been reported in a rs-fMRI study in chronic stroke patients.[33] This may be reflective of the adaptive reorganization of the sensorimotor network after large lesions.

Clinical recovery after experimental hemispherectomy was not only paralleled by increases in intraregional signal coherence and interregional functional connectivity in the contralateral hemisphere, but also with an overall enhanced functional clustering in the sensorimotor network. These changes, reflective of improved regional signal processing, may have been accomplished through (early) compensatory mechanisms such as recruitment or strengthening of latent but existing pathways in contralateral cortical and subcortical sensorimotor areas, but may also relate to structural neuronal plasticity.[34–37] For example, studies after unilateral stroke in rats have identified higher turnover rates of synaptic spines,[38] synaptogenesis, and dendritic growth [39] in the contralateral sensorimotor cortex.

There is previous evidence that ipsilateral projections are critically involved in early functional recovery after hemispherectomy in rats. Stimulation of the contralateral motor cortex after hemispherectomy has been shown to result in bilateral limb movement in phase with the time of functional recovery

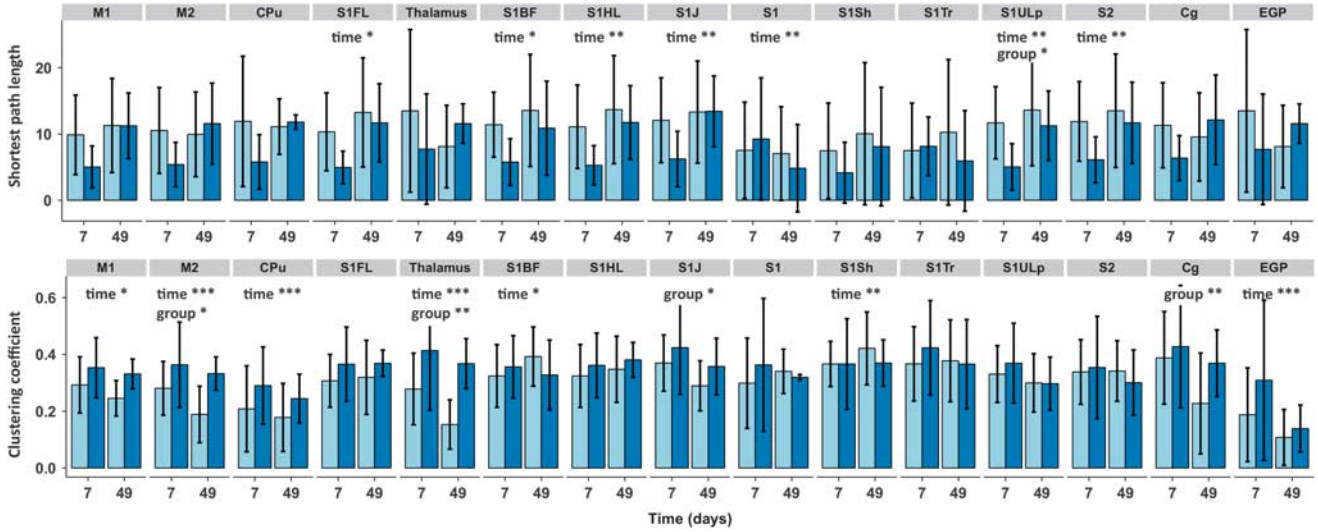

Figure 7. Contralateral sensorimotor network features for individual local nodes. Weighted shortest path length and clustering coefficient values for individual network nodes are shown at the top and bottom, respectively. Statistical node × group and node × time output from the nested multilevel analysis are shown for significant nodes only. Bars represent group mean ± s.d.; $^{*}P < 0.05$; $^{**}P < 0.01$; $^{***}P < 0.001$, versus controls. Cpu, caudate-putamen complex; M1, primary motor cortex; S1FL, primary somatosensory cortical forelimb area.

within 2 weeks.[6] Perhaps similar groups of neurons are responsible for contralateral, as well as ipsilateral innervation. Support for this hypothesis (i.e., an inborn structural capacity for bilateral innervation) is given by a study that demonstrated that cortical neuronal projections reach the bilateral thalamus in developing rat and cat brain.[40] Our functional network analysis revealed an increase in clustering of the contralateral thalamus with other network nodes (Figure 7). This increase, already present at 7 days after hemispherectomy, could well be indicative of the thalamus' role in ipsi and contralateral (sensori)motor control.

Our study has limitations. First, the reported functional connectivity measures are based on the correlation of low-frequency fluctuations of the BOLD signal, which is an indirect measure of synchronization of neuronal activities. It is important to note that interregional correlations do not provide information on the degree of local neuronal activity. Second, our study was limited to a few time points and did not include post mortem histology. As the largest changes in sensorimotor function occurred during the first week after hemispherectomy, measurement of structural and functional network changes at this early stage could contribute to the explanation of this rapid restoration of functions. In addition, post mortem histology could significantly aid in further understanding of the observed MRI-based changes.

In summary, our study sheds new light on patterns of changes in white matter integrity and functional connectivity in the contralateral brain after hemispherectomy in relation to change in sensorimotor function. These modifications may open avenues for the development of restorative interventions, such as non-invasive brain stimulation, that enhance the potential compensatory and restorative mechanisms toward functional recovery after hemispherectomy or large unilateral cerebrovascular injury.

AUTHOR CONTRIBUTIONS

WMO, MPAvM, KPJB, and RMD conceived and designed the experiments. WMO, MPAvM, PCvR, and PHG performed the experiments. MPAvM, PCvR, and PHG contributed reagents/materials/analysis tools. WMO and KvdM analyzed the data. WMO, KvdM, MPAvM, PCvR, PHG, KPJB, and RMD wrote the paper. WMO, KPJB, and RMD managed the running of the project.

DISCLOSURE/CONFLICT OF INTEREST

The authors declare no conflict of interest.

REFERENCES

1 Samargia SA, Kimberley TJ. Motor and cognitive outcomes in children after functional hemispherectomy. *Pediatr Phys Ther* 2009; **21**: 356–361.
2 van der Kolk NM, Boshuisen K, van Empelen R, Koudijs SM, Staudt M, van Rijen PC *et al.* Etiology-specific differences in motor function after hemispherectomy. *Epilepsy Res* 2013; **103**: 221–230.
3 Choi JT, Vining EP, Mori S, Bastian AJ. Sensorimotor function and sensorimotor tracts after hemispherectomy. *Neuropsychologia* 2010; **48**: 1192–1199.
4 Wakamoto H, Eluvathingal TJ, Makki M, Juhasz C, Chugani HT. Diffusion tensor imaging of the corticospinal tract following cerebral hemispherectomy. *J Child Neurol* 2006; **21**: 566–571.
5 Dijkhuizen RM, van der Marel K, Otte WM, Hoff EI, van der Zijden JP, van der Toorn A *et al.* Functional MRI and diffusion tensor imaging of brain reorganization after experimental stroke. *Transl Stroke Res* 2012; **3**: 36–43.
6 Machado AG, Shoji A, Ballester G, Marino R, Jr. Mapping of the rat's motor area after hemispherectomy: the hemispheres as potentially independent motor brains. *Epilepsia* 2003; **44**: 500–506.
7 Marino R Jr, Machado AG, Timo-Iaria C. Functional recovery after combined cerebral and cerebellar hemispherectomy in the rat. *Stereotact Funct Neurosurg* 2001; **76**: 83–93.
8 van der Zijden JP, Bouts MJ, Wu O, Roeling TA, Bleys RL, van der Toorn A *et al.* Manganese-enhanced MRI of brain plasticity in relation to functional recovery after experimental stroke. *J Cereb Blood Flow Metab* 2008; **28**: 832–840.
9 van Meer MP, Otte WM, van der Marel K, Nijboer CH, Kavelaars A, van der Sprenkel JW *et al.* Extent of bilateral neuronal network reorganization and functional recovery in relation to stroke severity. *J Neurosci* 2012; **32**: 4495–4507.
10 Breiman L. Random forests. *Mach Learn* 2001; **45**: 5–32.
11 Otte WM, van Meer MP, van der Marel K, Zwartbol R, Viergever MA, Braun KP *et al.* Experimental focal neocortical epilepsy is associated with reduced white matter volume growth: results from multiparametric MRI analysis. *Brain Struct Funct* 2013; **220**: 27–36.
12 Bullmore E, Sporns O. Complex brain networks: graph theoretical analysis of structural and functional systems. *Nat Rev Neurosci* 2009; **10**: 186–198.
13 Bernal-Rusiel JL, Greve DN, Reuter M, Fischl B, Sabuncu MR. Statistical analysis of longitudinal neuroimage data with Linear Mixed Effects models. *Neuroimage* 2012; **66C**: 249–260.
14 Johnston MV. Plasticity in the developing brain: implications for rehabilitation. *Dev Disabil Res Rev* 2009; **15**: 94–101.
15 Buonomano DV, Merzenich MM. Cortical plasticity: from synapses to maps. *Annu Rev Neurosci* 1998; **21**: 149–186.

16 Sterr A, Conforto AB. Plasticity of adult sensorimotor system in severe brain infarcts: challenges and opportunities. *Neural Plast* 2012; **2012**: 970136.
17 Burke MW, Kupers R, Ptito M. Adaptive neuroplastic responses in early and late hemispherectomized monkeys. *Neural Plast* 2012; **2012**: 852423.
18 Kennard MA. Reactions of monkeys of various ages to partial and complete decortication. *J Neuropathol Exp Neurol* 1944; **3**: 289.
19 Burke MW, Zangenehpour S, Ptito M. Partial recovery of hemiparesis following hemispherectomy in infant monkeys. *Neurosci Lett* 2010; **469**: 243–247.
20 Sullivan EV, Adalsteinsson E, Sood R, Mayer D, Bell R, McBride W *et al*. Longitudinal brain magnetic resonance imaging study of the alcohol-preferring rat. Part I: adult brain growth. *Alcohol Clin Exp Res* 2006; **30**: 1234–1247.
21 Yates MA, Juraska JM. Increases in size and myelination of the rat corpus callosum during adulthood are maintained into old age. *Brain Res* 2007; **1142**: 13–18.
22 Song SK, Sun SW, Ramsbottom MJ, Chang C, Russell J, Cross AH. Dysmyelination revealed through MRI as increased radial (but unchanged axial) diffusion of water. *Neuroimage* 2002; **17**: 1429–1436.
23 Chiang CW, Wang Y, Sun P, Lin TH, Trinkaus K, Cross AH *et al*. Quantifying white matter tract diffusion parameters in the presence of increased extra-fiber cellularity and vasogenic edema. *Neuroimage* 2014; **101**: 310–319.
24 Wang Y, Wang Q, Haldar JP, Yeh FC, Xie M, Sun P *et al*. Quantification of increased cellularity during inflammatory demyelination. *Brain* 2011; **134**: 3590–3601.
25 Wang X, Cusick MF, Wang Y, Sun P, Libbey JE, Trinkaus K *et al*. Diffusion basis spectrum imaging detects and distinguishes coexisting subclinical inflammation, demyelination and axonal injury in experimental autoimmune encephalomyelitis mice. *NMR Biomed* 2014; **27**: 843–852.
26 Chan KC, Khong PL, Lau HF, Cheung PT, Wu EX. Late measures of microstructural alterations in severe neonatal hypoxic-ischemic encephalopathy by MR diffusion tensor imaging. *Int J Dev Neurosci* 2009; **27**: 607–615.
27 Umesh Rudrapatna S, Wieloch T, Beirup K, Ruscher K, Mol W, Yanev P *et al*. Can diffusion kurtosis imaging improve the sensitivity and specificity of detecting microstructural alterations in brain tissue chronically after experimental stroke? Comparisons with diffusion tensor imaging and histology. *Neuroimage* 2014; **97**: 363–373.
28 van der Zijden JP, van der Toorn A, van der Marel K, Dijkhuizen RM. Longitudinal *in vivo* MRI of alterations in perilesional tissue after transient ischemic stroke in rats. *Exp Neurol* 2008; **212**: 207–212.
29 Clancy B, Darlington RB, Finlay BL. Translating developmental time across mammalian species. *Neuroscience* 2001; **105**: 7–17.
30 Chan KC, Kancherla S, Fan SJ, Wu EX. Long-term effects of neonatal hypoxia-ischemia on structural and physiological integrity of the eye and visual pathway by multimodal MRI. *Invest Ophthalmol Vis Sci* 2014; **56**: 1–9.
31 van Meer MP, van der Marel K, Otte WM, Berkelbach van der Sprenkel JW, Dijkhuizen RM. Correspondence between altered functional and structural connectivity in the contralesional sensorimotor cortex after unilateral stroke in rats: a combined resting-state functional MRI and manganese-enhanced MRI study. *J Cereb Blood Flow Metab* 2010; **30**: 1707–1711.
32 van Meer MP, van der Marel K, Wang K, Otte WM, El Bouazati S, Roeling TA *et al*. Recovery of sensorimotor function after experimental stroke correlates with restoration of resting-state interhemispheric functional connectivity. *J Neurosci* 2010; **30**: 3964–3972.
33 Wang L, Yu C, Chen H, Qin W, He Y, Fan F *et al*. Dynamic functional reorganization of the motor execution network after stroke. *Brain* 2010; **133**: 1224–1238.
34 Chen R, Cohen LG, Hallett M. Nervous system reorganization following injury. *Neuroscience* 2002; **111**: 761–773.
35 Villablanca JR, Hovda DA. Developmental neuroplasticity in a model of cerebral hemispherectomy and stroke. *Neuroscience* 2000; **95**: 625–637.
36 Holt RL, Mikati MA. Care for child development: basic science rationale and effects of interventions. *Pediatr Neurol* 2011; **44**: 239–253.
37 Caroni P, Donato F, Muller D. Structural plasticity upon learning: regulation and functions. *Nat Rev Neurosci* 2012; **13**: 478–490.
38 Takatsuru Y, Fukumoto D, Yoshitomo M, Nemoto T, Tsukada H, Nabekura J. Neuronal circuit remodeling in the contralateral cortical hemisphere during functional recovery from cerebral infarction. *J Neurosci* 2009; **29**: 10081–10086.
39 Jones TA, Kleim JA, Greenough WT. Synaptogenesis and dendritic growth in the cortex opposite unilateral sensorimotor cortex damage in adult rats: a quantitative electron microscopic examination. *Brain Res* 1996; **733**: 142–148.
40 Molinari M, Minciacchi D, Bentivoglio M, Macchi G. Efferent fibers from the motor cortex terminate bilaterally in the thalamus of rats and cats. *Exp Brain Res* 1985; **57**: 305–312.

Supplementary Information accompanies the paper on the Journal of Cerebral Blood Flow & Metabolism website (http://www.nature.com/jcbfm)